



# Ligand substitution in the osmium carbonyl cluster $\text{Os}_2(\text{CO})_8(\mu_3\text{-SbPh})\text{Os}(\text{CO})_3(\text{Cl})_2$ : Towards derivatives of the osmostibine metalloligand

Ying-Zhou Li<sup>a,\*</sup>, Zhi-Rui Yuan<sup>a</sup>, Rakesh Ganguly<sup>b,c</sup>, Yongxin Li<sup>b</sup>, Deborah Roshni Rajaratnam<sup>b</sup>, Weng Kee Leong<sup>b,\*</sup>

<sup>a</sup>Shandong Provincial Key Laboratory of Molecular Engineering, Qilu University of Technology (Shandong Academy of Science), Ji'nan 250353, PR China

<sup>b</sup>Division of Chemistry & Biological Chemistry, Nanyang Technological University, 21 Nanyang Link, 637371, Singapore

<sup>c</sup>NH91, Tehsil Dadri, Greater Noida, Gautam Buddha Nagar, Shiv Nadar University, 201314, India

## ARTICLE INFO

### Article history:

Received 8 March 2021

Revised 3 April 2021

Accepted 5 April 2021

Available online 23 April 2021

### Keywords:

Osmostibine

Osmium

Antimony

Metalloligand

Phosphine

Carbonyl clusters

## ABSTRACT

Derivatisation of the osmium carbonyl cluster  $\text{Os}_2(\text{CO})_8(\mu_3\text{-SbPh})\text{Os}(\text{CO})_3(\text{Cl})_2$ , **1**, the precursor to the metalloligand  $\text{Os}_2(\text{CO})_8(\mu\text{-SbPh})$ , **2**, was explored as a route to derivatives of the latter. The reaction of **1** with  $\text{PPh}_3$  in different stoichiometries and under trimethylamine N-oxide activation in  $\text{CH}_3\text{CN}$  led to mono-, di-, tri- and tetra-substitution by  $\text{PPh}_3$  and  $\text{CH}_3\text{CN}$ . The first substitution occurred at the  $\text{Os}(\text{CO})_3\text{Cl}_2$  “spike” and although subsequent substitution favoured  $\text{CH}_3\text{CN}$  at the osmostibine moiety, the latter was not readily displaced by  $\text{PPh}_3$ . Substitution at the “spike” also shut down release of the substituted osmostibine. The  $\text{CH}_3\text{CN}$ -substituted osmostibine could, however, be generated *in situ* through the bis-acetonitrile derivative of **1** by conversion of the  $\text{Os}(\text{CO})_2(\text{NCCH}_3)\text{Cl}_2$  “spike” back into its removable  $\text{Os}(\text{CO})_3\text{Cl}_2$  form through reaction with CO gas, and was then trapped with  $\text{W}(\text{CO})_5(\text{NCCH}_3)$ .

© 2021 Elsevier B.V. All rights reserved.

## 1. Introduction

A metalloligand may refer to a ligand comprising a coordination complex in which the metal directs secondary donor sites residing on peripheral organic moieties, to suitably orientate them for coordination to other metal centres. The metalloligand coordination strategy has long been exploited to synthesize a wide range of heterometallic complexes, clusters, and coordination polymers [1]. Another type of metalloligands have their metal centres directly coordinated to a second metal centre to form an  $\text{M} \rightarrow \text{M}'$  Lewis pair [2]. They are more usually employed to introduce a main group metal into organometallic compounds, and the direct  $\text{E} \rightarrow \text{M}$  or  $\text{E} \leftarrow \text{M}$  ( $\text{E}$  = main group metal,  $\text{M}$  = transition metal) interaction imbues distinct electronic properties which are not so readily available with organic ligands [3].

We previously reported that the unique metalloligand, the osmostibine  $\text{Os}_2(\text{CO})_8(\mu\text{-SbPh})$ , **2**, may be obtained by stirring the precursor cluster  $\text{Os}_2(\text{CO})_8(\mu_3\text{-SbPh})\text{Os}(\text{CO})_3(\text{Cl})_2$ , **1**, in  $\gamma\text{-Al}_2\text{O}_3$  (Scheme 1) [4]. Given that organostibines and its derivatives are often employed as L- or Z-type metalloligands to tune the catalytic

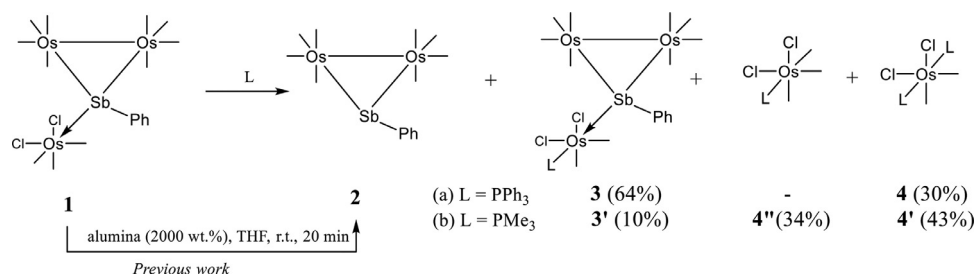
activity of transition metal centers [5], a metallostibine such as **2** is thus of interest. It can be viewed as a dual  $\text{Os}(\text{CO})_4$ -stabilized stibinidene, and we have shown that it has a strong electron-donating ability that is comparable to that of alkyl phosphines. It is a versatile metalloligand, allowing the simultaneous introduction of the transition metal Os and the main group metal Sb onto another metal complex/cluster [6]. Such metallostibine donor ligands are rare [7], and hence it is desirable if the two  $\text{Os}(\text{CO})_4$  moieties in **2** can be modified to allow for fine-tuning of its electronic properties. The highly nucleophilic nature of **2** made direct functionalization difficult and hence we explored the derivatization of **1**, which may be regarded as a “protected” synthetic equivalent for **2**, as a possible route forward.

## 2. Results and discussion

As reported previously,  $\text{PMe}_3$  attacked the  $\text{Os}(\text{CO})_3\text{Cl}_2$  “spike” in **1** at room temperature to displace the osmostibine **2** [4b]. In a re-examination of this reaction, a new monosubstituted derivative of **1**, viz.,  $\text{Os}_2(\text{CO})_8(\mu_3\text{-SbPh})\text{Os}(\text{CO})_2(\text{PMe}_3)\text{Cl}_2$ , **3'**, was also identified as a minor product. The analogous reaction with  $\text{PPh}_3$  did not proceed at room temperature, presumably due to the weaker nucleophilicity of  $\text{PPh}_3$ ; at elevated temperature it afforded the analogue of **3'**, viz.,  $\text{Os}_2(\text{CO})_8(\mu_3\text{-SbPh})\text{Os}(\text{CO})_2(\text{PPh}_3)\text{Cl}_2$ , **3**, as

\* Corresponding authors.

E-mail address: [chmlwk@ntu.edu.sg](mailto:chmlwk@ntu.edu.sg) (W.K. Leong).



**Scheme 1.** Direct ligand substitution reaction of **1** with phosphines. Reaction conditions: (a) PMe<sub>3</sub> (1.5 equiv.), THF, r.t., 36 h; (b) PPh<sub>3</sub> (1.1 equiv.), THF, 60 °C, 6 h. Yields of **2** were not determined as it decomposed on silica.

**Table 1**

Common atom labeling scheme and selected bond lengths (Å) and angles (°) for clusters **1**, **3** and **3'**. Each has two crystallographically independent molecules.

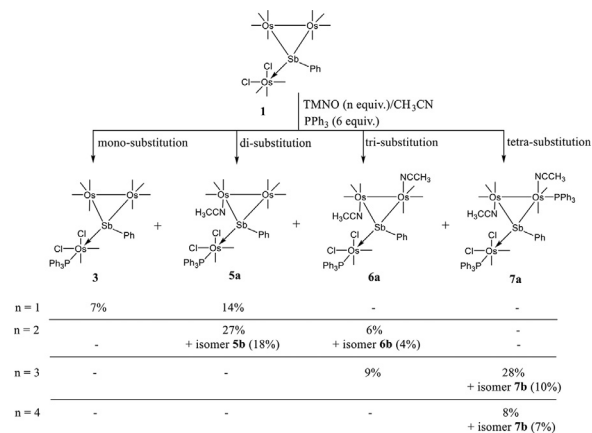
	1 <sup>a</sup>		3		3'	
Os1-Os2	2.9504(6)	2.9612(6)	2.9467(4)	2.9457(4)	2.950(1)	2.948(1)
Os1-Sb	2.6668(7)	2.6500(8)	2.6791(3)	2.6805(4)	2.680(1)	2.665(1)
Os2-Sb	2.6582(7)	2.6512(7)	2.6856(5)	2.6615(4)	2.660(1)	2.681(1)
Os3-Sb	2.6882(8)	2.6795(8)	2.6734(5)	2.6699(5)	2.667(1)	2.666(1)
Os3-CO(1) <sup>b</sup>	3.043	3.033	3.021	3.015	3.03	3.01
Os3-CO(2) <sup>b</sup>	3.021	3.023	3.010	2.943	3.02	3.00
Os1-Sb-Os2	67.293(18)	67.917(19)	66.63(1)	66.93(1)	67.06(3)	66.92(3)
Os2-Sb-Os3	132.29(2)	132.05(3)	131.32(2)	134.91(2)	130.13(5)	130.40(5)
Os1-Sb-Os3	123.88(3)	125.53(3)	127.42(2)	125.10(2)	131.22(5)	129.63(5)

<sup>a</sup> Data from ref. [5a]. <sup>b</sup> Sum of Os-C and C-O bond lengths.

the major product and a minor amount of Os(CO)<sub>2</sub>(PPh<sub>3</sub>)<sub>2</sub>Cl<sub>2</sub>, **4** (Scheme 1). These results suggest an associative mechanism for phosphine substitution at the Os(CO)<sub>3</sub>Cl<sub>2</sub> "spike".

The molecular structures of **3**, **3'** and **4** have been established by X-ray crystallographic studies; an ORTEP plot showing the molecular structure of **3** is given in Fig. 1, and selected bond parameters, together with a common atomic numbering scheme for **1**, **3** and **3'**, are collected in Table 1. In both **3** and **3'**, the phosphine ligand is *trans* to the osmostibine moiety. This suggests that the CO ligand *trans* to the osmostibine moiety in **1** is preferentially labilised and is consistent with the expected greater *trans* effect of osmostibine over Cl. Interestingly, the Os3-Sb bond length shortens in going from **1** ( $\geq 2.68$  Å) to **3** ( $\sim 2.67$  Å) and **3'** ( $< 2.67$  Å). This trend is the reverse of that expected from the increasing  $\sigma$ -donor ability but is correlated with the decreasing  $\pi$ -acceptor ability, in moving from CO to PPh<sub>3</sub> to PMe<sub>3</sub>. It is thus indicative of a  $\pi$ -interaction involving the osmostibine and Os3. A natural bond orbital (NBO) analysis on **3'** gave Wiberg bond indices of  $\sim 0.70$  and  $0.71$  for the two Os-Sb bonds in the osmostibine fragment, and  $\sim 0.72$  for the coordinative Os-Sb bond, consistent with the presence of a weak  $\pi$  back-donation in the latter. In comparison with the bridging [SbPh<sub>2</sub>]<sup>-</sup> ligand, however, the osmostibine has a weaker *trans* effect [8].

The direct reaction of **1** with phosphines, even in the presence of a large excess of the latter and a prolonged reaction time, did not result in any substitution at the osmostibine fragment. Presumably, the two Cl ligands on the Os(CO)<sub>3</sub>Cl<sub>2</sub> "spike" fragment make that Os center more susceptible to nucleophilic attack by the phos-



**Scheme 2.** TMNO activated substitution reactions of **1** with PPh<sub>3</sub>.

phines. The CO ligands on this fragment may also be expected to be more reactive towards nucleophilic Me<sub>3</sub>NO (TMNO) [9], and so we next examined the derivatization of **1** through TMNO-activated substitution with PPh<sub>3</sub>. Our attempts at this with excess phosphine and various equivalents of TMNO are summarized in Scheme 2.

With one equivalent of TMNO, even with dropwise addition, di-substitution to form Os<sub>2</sub>(CO)<sub>7</sub>(CH<sub>3</sub>CN)( $\mu_3$ -SbPh)Os(CO)<sub>2</sub>(PPh<sub>3</sub>)Cl<sub>2</sub>, **5**, was observed to be preferred over the formation of **3**, suggesting that the latter was more substitutionally labile than the parent cluster **1**. For the di-substitution product **5**, the second substitution

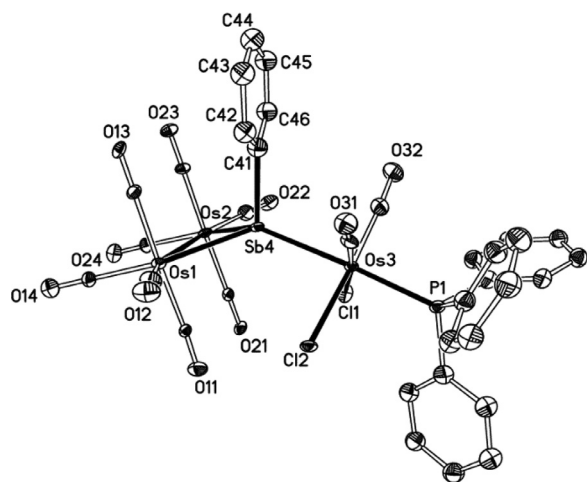


**Fig. 1.** ORTEP plot showing the molecular structure of **3**. Thermal ellipsoids are drawn at the 50% probability level. Organic hydrogen atoms are omitted for clarity.

is most probably by a  $\text{CH}_3\text{CN}$  ligand at an axial position of the osmostibine; this is energetically more favorable than an equatorial position which would place two strongly  $\pi$ -accepting CO ligands mutually *trans* [10]. There are four possible diastereoisomers for **5**, assuming free rotation about the Sb–“spike” bond (Fig. 3). The di-substitution product isolated from this reaction corresponds to isomer **5a**, which is the most energetically favoured stereoisomer based on DFT calculations. The molecular structure of **5a** has also been confirmed by a single-crystal X-ray diffraction study; an OR-

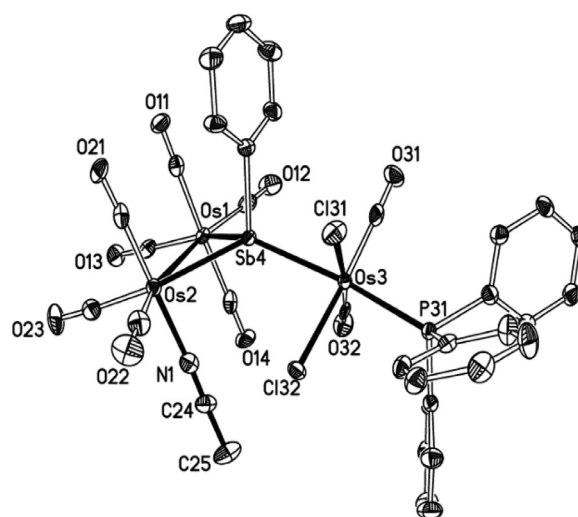


**Fig. 2.** ORTEP plot showing the molecular structure of **5a**. Hydrogen atoms are omitted for clarity. Thermal ellipsoids are drawn at the 50% probability level. Selected bond lengths (Å) and angles ( $^\circ$ ): Os1–Os2 = 2.9368(4); Os1–Sb4 = 2.7005(4); Os2–Sb4 = 2.6660(5); Os3–Sb4 = 2.6779(4); Os3–Sb4–Os1 = 131.790(16); Os2–Sb4–Os3 = 129.069(16); Os2–Sb4–Os1 = 66.353(12).

TEP plot showing the molecular structure and selected bond parameters are shown in Fig. 2.

As anticipated, cluster **5a** was the major product isolated from the reaction with two equivalents of TMNO. The mass spectrum of a second product isolated was similar to that for **5a**, with a cluster of peaks at  $m/z$  1415 which corresponded to an  $[\text{M}+\text{H}_2\text{O}]^+$

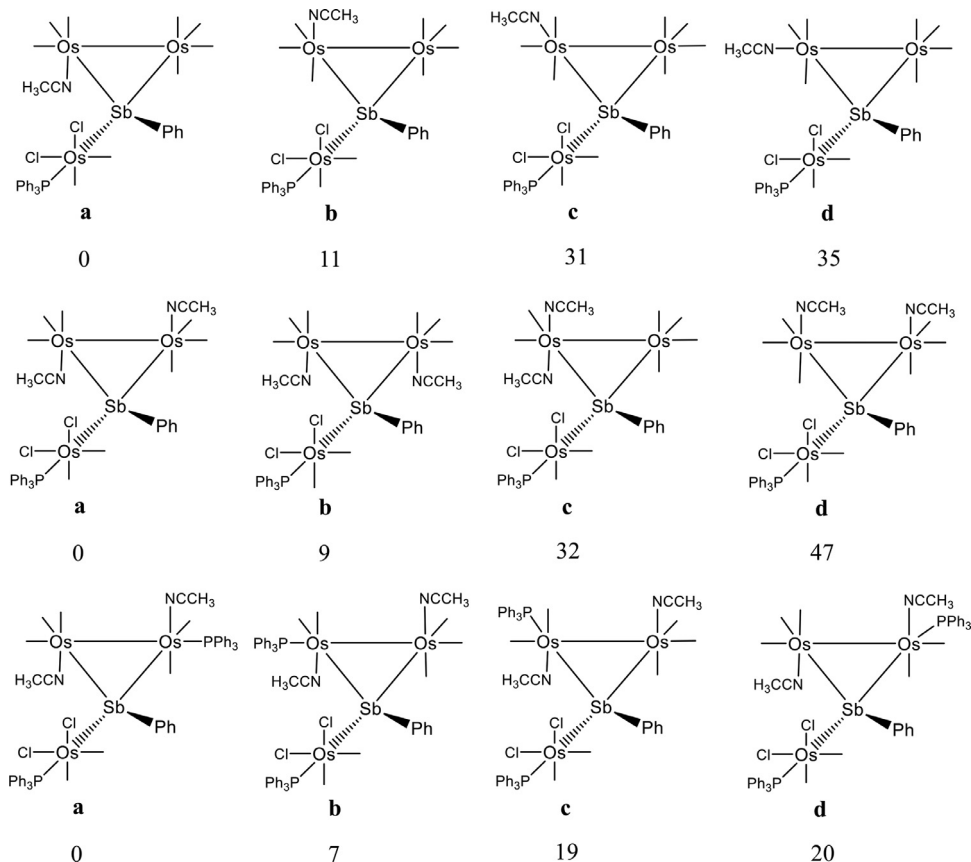


**Fig. 3.** The isomers of **5** (top), **6** (middle) and **7** (bottom) which have been studied computationally. The Gibbs free energies (kJ/mol) relative to the most stable isomer are given below each structure.

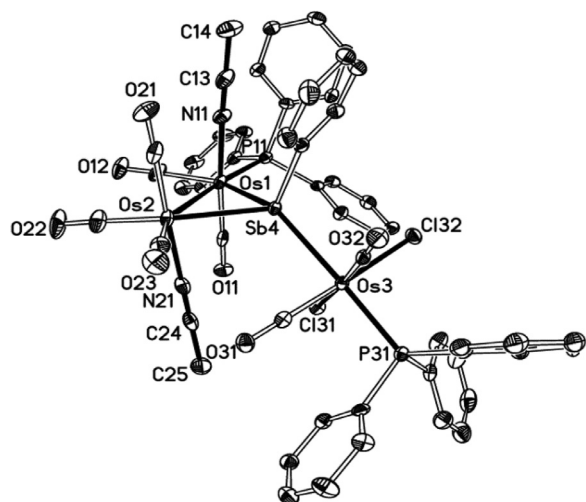


**Fig. 4.** ORTEP plot showing the molecular structure of **7a**. Hydrogen atoms are omitted for clarity. Thermal ellipsoids are drawn at the 50% probability level. Selected bond lengths (Å) and angles (°): Os1–Os2 = 2.9122(3); Os1–Sb4 = 2.6842(4); Os2–Sb4 = 2.6814(3); Os3–Sb4 = 2.7081(4); Os3–Sb4–Os1 = 137.303(13); Os2–Sb4–Os3 = 119.164(13); Os2–Sb4–Os1 = 65.744(9).

ion. Its  $^1\text{H}$  NMR spectrum was also similar, with a singlet  $\text{CH}_3\text{CN}$  resonance at  $\delta$  2.18 ppm (*cf.*,  $\delta$  1.44 ppm for **5a**). We ruled out an isomer with an equatorial  $\text{CH}_3\text{CN}$ ; a previous crystallographically characterized example with such a moiety was stable only in  $\text{CH}_3\text{CN}$  as solvent, and the proton resonance for the ligand was not observed due to fast exchange with the solvent ( $\text{CD}_3\text{CN}$ ) [8]. DFT calculations suggest that the second most stable isomer after **5a** is that with an axial  $\text{CH}_3\text{CN}$  *syn* to the Sb–Ph group, *viz.*, **5b** (Fig. 3). We have thus tentatively assigned this second product to be **5b**; the downfield shift of the *syn*- $\text{CH}_3\text{CN}$  proton resonance relative to the *anti*- $\text{CH}_3\text{CN}$  in **5a** may be due to through-space deshielding by the adjacent *syn*-phenyl ring [11].

Apart from **5a** and **5b**, two minor products were also isolated from this reaction. Their  $^1\text{H}$  NMR spectra clearly showed two singlet resonances ascribable to  $\text{CH}_3\text{CN}$  ligands; their mass spectra also showed a cluster of peaks at  $m/z$  1428 assignable to the  $[\text{M}+\text{H}_2\text{O}]^+$  ion. They are thus proposed to be tri-substituted products with the formulation  $\text{Os}_2(\text{CO})_6(\text{CH}_3\text{CN})_2(\mu_3\text{-SbPh})\text{Os}(\text{CO})_2(\text{PPh}_3)\text{Cl}_2$ , **6**. Assuming that the geometry about the “spike” is the same as in **3** and **5**, and the two  $\text{CH}_3\text{CN}$  ligands occupy axial positions on the osmostibine, there are four possible isomers for **6** (Fig. 3). The one with proton resonances at  $\delta$  1.42 and 2.26 ppm, probably corresponding to *anti*- and *syn*- $\text{CH}_3\text{CN}$ , respectively, is tentatively assigned as isomer **6a**; this is the most energetically favored stereoisomer based on DFT calculations. The other product exhibited two singlet resonances at  $\delta$  1.45 and 1.54 ppm, values which are closer to that for **5b** (1.44 ppm) and hence suggesting that both  $\text{CH}_3\text{CN}$  ligands are likely in axial positions and *anti* to the Sb–Ph group. We have tentatively identified it as isomer **6b** (Fig. 3); that the two *anti*- $\text{CH}_3\text{CN}$  ligands are not chemically equivalent may be ascribed to strong hydrogen bonding interactions with the Cl ligands in the “spike”, impeding its free rotation about the Os–Sb bond (Figure S3).

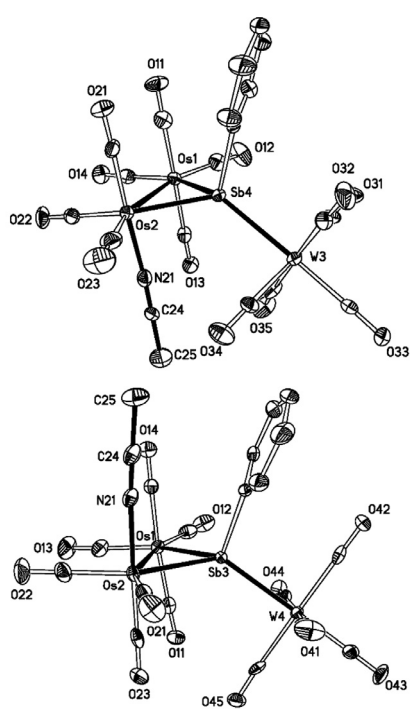
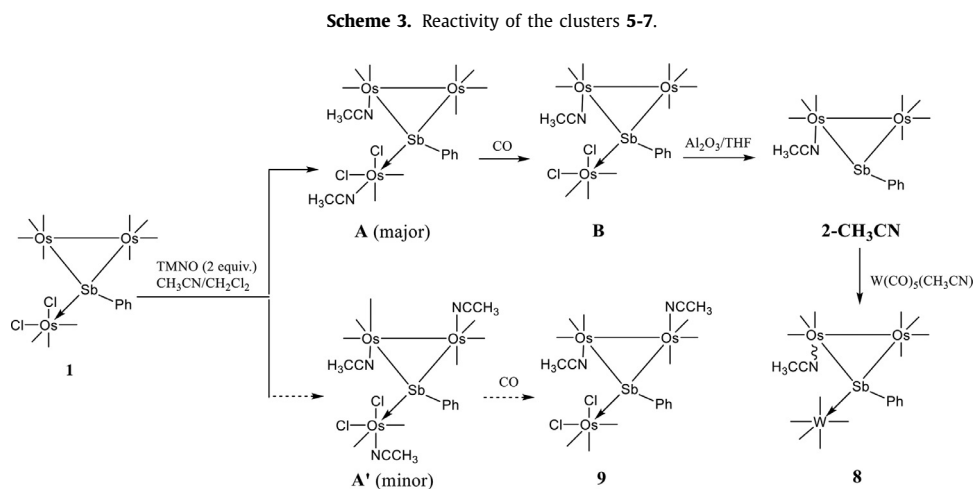
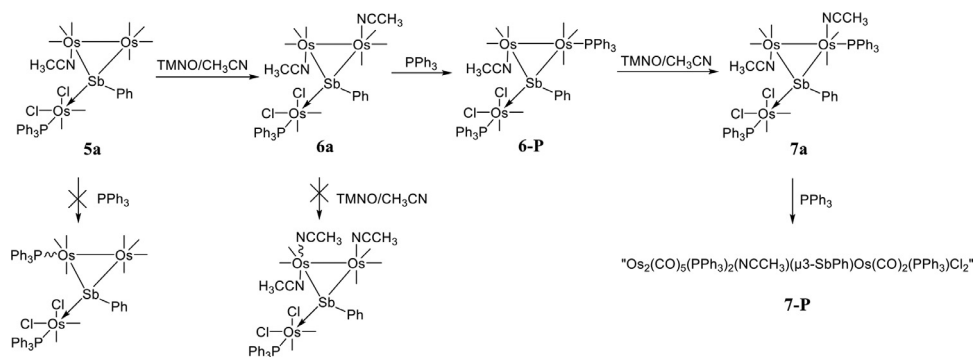
With three equivalents of TMNO, the tri-substitution isomer **6b** was not observed although isomer **6a** was obtained as a minor product. Instead, the two major products appeared to be isomers of tetra-substitution, *viz.*,  $\text{Os}_2(\text{CO})_5(\text{PPh}_3)(\text{CH}_3\text{CN})_2(\mu_3\text{-SbPh})\text{Os}(\text{CO})_2(\text{PPh}_3)\text{Cl}_2$ , **7**, as both showed the molecular ion at  $m/z$  of 1644 in their mass spectra. A computational study on the four diastereoisomers derived from the most energetically favored di-substitution cluster **6a** are listed in Fig. 3, and the most stable iso-

mer is **7a**, which corresponds to that characterized structurally by a single-crystal X-ray diffraction study; the ORTEP plot is given in Fig. 4 together with selected bond parameters.

The second product has been tentatively assigned to be **7b**, the next most stable isomer. Their  $^1\text{H}$  NMR spectra are in accord with these assignments; both showed two sets of resonances for the  $\text{CH}_3\text{CN}$  ligands, at  $\delta$  1.32 and 1.68 ppm for **7a**, and  $\delta$  0.91 and 2.31 ppm for **7b**, which corresponded to the ligands *anti*- and *syn* to the Sb–Ph group, respectively. The resonance for the  $\text{CH}_3\text{CN}$  ligand attached to the same osmium centre as the phosphine was shifted upfield with respect to that of **6a** ( $\delta$  1.42 and 2.26 ppm for *anti*- and *syn*, respectively), and doublets due to long-range P–H coupling ( $^5J_{\text{PH}} \sim 0.8$  Hz) [12]. An attempt to increase the yields of these tetra-substitution products through increasing the amount of TMNO to four equivalents afforded instead lower yields of **7a** and **7b**; presumably, more substituted derivatives were formed which were less stable and hence not amenable to chromatographic separation. This apparent preference for tetra- over tri-substitution suggests that the latter are more substitutionally labile than the parent di-substituted clusters, and is consistent with the observations with one equivalent of TMNO.

The reactivity of clusters **5–7** with respect to nucleophilic replacement of the  $\text{CH}_3\text{CN}$  ligands was investigated mainly by mass spectrometry, given the complexity of the reactions and relatively low yields of products; the results are summarized below (Scheme 3). Attempts at generating a  $\text{CH}_3\text{CN}$ -substituted osmostibine from **5a** by stirring with  $\gamma$ -alumina or  $\text{PMe}_3$  for 70 h failed (as judged spectroscopically), and may be ascribed to the reduced electrophilicity of the  $\text{Os}(\text{CO})_2(\text{PPh}_3)\text{Cl}_2$  moiety compared to the  $\text{Os}(\text{CO})_3\text{Cl}_2$  moiety in **1**. Displacement of the  $\text{CH}_3\text{CN}$  ligand with excess  $\text{PPh}_3$  or  $\text{PMe}_3$  also did not proceed even when heated at  $65^\circ\text{C}$  for 20 h, although it readily converted to **6a** in the presence of one equivalent of TMNO in  $\text{CH}_3\text{CN}$  solution. In contrast, cluster **6a** did not undergo further TMNO-activated substitution of CO with  $\text{CH}_3\text{CN}$  but although it was relatively stable under ambient conditions and tolerated silica gel separation, it underwent ready substitution of one of its  $\text{CH}_3\text{CN}$  ligands by  $\text{PPh}_3$  to afford a new tri-substituted cluster  $\text{Os}_2(\text{CO})_6(\text{PPh}_3)(\text{CH}_3\text{CN})(\mu_3\text{-SbPh})\text{Os}(\text{CO})_2(\text{PPh}_3)\text{Cl}_2$ , **6-P**. The identity is based on the observation of cluster of peaks at  $m/z$  1631 and 1649, which are assignable to the  $[\text{M}]^+$  and  $[\text{M}+\text{H}_2\text{O}]^+$  ions, respectively (Figure S17). The proposed structure depicted in Scheme 3 is the most thermodynamically stable from a DFT computation carried out on eight possible isomers with an axial  $\text{CH}_3\text{CN}$  and an equatorial  $\text{PPh}_3$  on the osmostibine fragment (Figure S22). Compared to **6a**, it is more susceptible to one more  $\text{CH}_3\text{CN}$  substitution to give **7a**; consistent with this is the experimental observation that the main products from the substitution reaction of **1** with three equivalents of TMNO were not the tri-substituted products **6**, but rather the tetra-substituted products **7**. Cluster **7a** could similarly undergo substitution of one of its  $\text{CH}_3\text{CN}$  ligands with  $\text{PPh}_3$  at room temperature to afford a new tetra-substituted derivative  $\text{Os}_2(\text{CO})_5(\text{PPh}_3)_2(\text{CH}_3\text{CN})(\mu_3\text{-SbPh})\text{Os}(\text{CO})_2(\text{PPh}_3)\text{Cl}_2$ , **7-P**; the chemical formulation of **7-P** is corroborated by the mass spectrum (Figure S17).

From the above, there are several observations that may be made concerning TMNO-activated substitution in **1** and its derivatives: (a) The first substitution in **1** is of the CO *trans* to the osmostibine; it is the only carbonyl ligand on the “spike” that undergoes substitution. (b) Subsequent substitution is at the osmostibine, although it appears that each osmium centre cannot accommodate more than one acetonitrile ligand. (c) Only one of the acetonitrile ligands can be substituted by  $\text{PPh}_3$ . These observations suggested an alternative approach to derivatize the osmostibine; the bis-acetonitrile derivative **A** was generated from **1** and then reacted *in situ* with CO gas to form the mono-acetonitrile deriva-



	Os1-Os2	Os1-Sb	Os2-Sb	Sb-W	Os2-Sb-Os1	W-Sb-Os2	W-Sb-Os1
<b>8a</b>	2.9392(4)	2.6911(5)	2.6622(5)	2.7954(5)	66.60(1)	127.48(2)	130.32(2)
<b>8b</b>	2.9493(3)	2.6848(4)	2.6656(4)	2.7592(4)	66.90(1)	132.14(2)	127.29(1)

**Fig. 5.** ORTEP plots showing the molecular structures of **8a** (top) and **8b** (bottom), and table of selected bond lengths (Å) and angles (°). Hydrogen atoms have been omitted and the thermal ellipsoids are drawn at the 50% probability level.

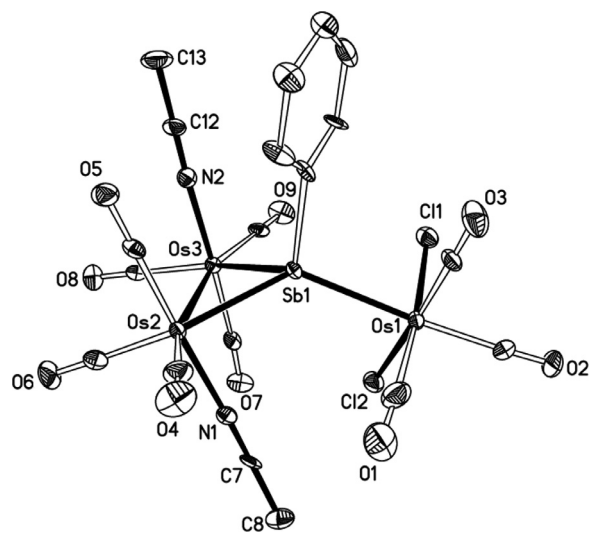


**Fig. 6.** ORTEP plot showing the molecular structure of **9**. Thermal ellipsoids are drawn at the 50% probability level. Organic hydrogen atoms are omitted for clarity. Selected bond lengths (Å) and angles (°): Os2-Os3 = 2.9369(6); Os2-Sb1 = 2.6444(8); Os3-Sb1 = 2.6539(8); Os1-Sb1 = 2.6820(8); Os3-N2 = 2.08(1); Os2-N1 = 2.10(1); Os1-Cl1 = 2.422(3); Os1-Cl2 = 2.429(3); Os3-Sb1-Os2 = 67.33(2); Sb1-Os2-Os3 = 56.49(2); Os2-Os3-Sb1 = 56.18(2); Os1-Sb1-Os2 = 129.34(3); Os1-Sb1-Os3 = 128.75(3).

tive **B** which released the Os(CO)<sub>3</sub>Cl<sub>2</sub> moiety readily to give the mono-acetonitrile osmostibine **2-CH<sub>3</sub>CN**. The latter was trapped by reaction with W(CO)<sub>5</sub>(NCCH<sub>3</sub>) to afford two isomeric clusters Os<sub>2</sub>(CO)<sub>7</sub>(CH<sub>3</sub>CN)(μ<sub>3</sub>-SbPh)W(CO)<sub>5</sub>, **8a** and **8b** (Scheme 4).

The structures of **8a** and **8b** have been confirmed crystallographically; they differ in the orientation of the CH<sub>3</sub>CN ligand (Fig. 5). A minor side product isolated from the reaction, and only characterized crystallographically, was cluster **9** which probably resulted from a tris-acetonitrile derivative **A'** (Fig. 6). The isolation of **9** is further evidence for the substitution of CH<sub>3</sub>CN by CO in the transformation from **A** to **B**; the presence of the latter was also verified by the mass spectrum of the reaction mixture (Figure S18). A DFT computational study carried out on **2-CH<sub>3</sub>CN** and a hypothetical di-PPh<sub>3</sub> substituted osmostibine derivative, viz., Os<sub>2</sub>(CO)<sub>6</sub>(PPh<sub>3</sub>)<sub>2</sub>(μ-SbPh) (**2-diPPh<sub>3</sub>**), shows that the HOMO energy levels follow the trend: **2-diPPh<sub>3</sub>** (-5.17 eV) > **2-CH<sub>3</sub>CN** (-5.61 eV) > **2** (-6.07 eV), suggesting that the electron donating ability of **2** can be tuned through CO ligand substitution (Figure S24).

### 3. Conclusion

In this work, we examined the substitution of **1** with CH<sub>3</sub>CN and PPh<sub>3</sub> as potential precursors to derivatives of the metallostibine **2**. A number of di-, tri- and tetra-substituted derivatives were isolated and characterized, but initial substitution was found to occur at one of the carbonyl ligands on the "spike" which effectively prevented generation of the osmostibine. The generation of a bis-acetonitrile substituted derivative of **1**, followed by carbonylation of the CH<sub>3</sub>CN-substituted "spike" back into its original Os(CO)<sub>3</sub>Cl<sub>2</sub> form and then its removal with γ-Al<sub>2</sub>O<sub>3</sub>, has proven to be a feasible route to CH<sub>3</sub>CN-substituted osmostibine. Nevertheless, a more facile route to osmostibine derivatives is still desirable.

### 4. Experimental

**General procedure.** All reactions were performed under an argon atmosphere with standard Schlenk techniques. Reagent grade solvents were dried by the standard procedures and were freshly distilled prior to use. Cluster **1** and complex W(CO)<sub>5</sub>(CH<sub>3</sub>CN) were prepared according to literature methods [4b,13]; all other chemicals were from commercial sources and used as supplied. γ-Al<sub>2</sub>O<sub>3</sub> (neutral, Brockmann activity I, 150 mesh, 58 Å) was purchased from Sigma-Aldrich and used as received without further activation. TLC separations were carried out on 20 × 20 cm<sup>2</sup> plates coated with silica gel 60 F254 from Merck. NMR spectra were recorded on a Bruker BBFO1 or Avance III 400 MHz NMR spectrometer at room temperature. All <sup>1</sup>H chemical shifts were referenced to the residual proton resonance; <sup>31</sup>P chemical shifts were referenced to external 85% aq. H<sub>3</sub>PO<sub>4</sub>. Mass spectra were recorded in ESI-ToF mode on a Waters UPLC-Q-ToF instrument. Elemental analyses were carried out on a Eurovector EA3000 analyser.

**Reaction of 1 with PMe<sub>3</sub>.** Cluster **1** (20 mg, 17 μmol) was dissolved in dry THF (8 ml), followed by the addition of PMe<sub>3</sub> (2.0 mg, 25 μmol). The resulting light yellow mixture was stirred at room temperature for 36 h and IR monitoring showed **1** was completely consumed. The solvent was then removed, and the residue separated by TLC on silica with CH<sub>2</sub>Cl<sub>2</sub>/hexane (3:1, v/v) as the eluent to give three separable bands. The first two colorless bands were identified as the known Os(CO)<sub>2</sub>(PMe<sub>3</sub>)<sub>2</sub>Cl<sub>2</sub>, **4'** (R<sub>f</sub> = 0.50; 3.5 mg, 43%), and Os(CO)<sub>3</sub>(PMe<sub>3</sub>)Cl<sub>2</sub>, **4''** (R<sub>f</sub> = 0.35; 2.5 mg, 34%), respectively.

The third very light yellow band was identified as Os<sub>3</sub>(CO)<sub>10</sub>(PMe<sub>3</sub>)(SbPh)Cl<sub>2</sub>, **3'** (R<sub>f</sub> = 0.15; 2.0 mg, 10%). IR (CH<sub>2</sub>Cl<sub>2</sub>): ν(CO) 2132m, 2096s, 2051vs, 2030vs, 1959s cm<sup>-1</sup>. <sup>1</sup>H NMR (C<sub>6</sub>D<sub>6</sub>) δ 7.42 (d, 2H, Ph-H), 7.03 (t, 2H, Ph-H), 6.93 (t, 1H, Ph-H). <sup>31</sup>P{<sup>1</sup>H} NMR (C<sub>6</sub>D<sub>6</sub>) δ -34.6 ppm. Anal. Calcd for C<sub>19</sub>H<sub>14</sub>Cl<sub>2</sub>O<sub>10</sub>Os<sub>3</sub>PSb: C 19.07, H 1.18. Found: C 18.94, H 1.42. ESI-MS<sup>+</sup> (m/z): 1216 [M+H<sub>2</sub>O]<sup>+</sup>, 1188 [M+H<sub>2</sub>O-CO]<sup>+</sup>.

**Reaction of 1 and PPh<sub>3</sub>.** Cluster **1** (20 mg, 17 μmol) was dissolved in dry THF (8 ml), followed by the addition of PPh<sub>3</sub> (5.0

mg, 19 μmol). The resulting light yellow mixture was heated at 60 °C for 6 h and IR monitoring showed **1** was completely consumed. The solvent was then removed and the residue separated by TLC on silica with CH<sub>2</sub>Cl<sub>2</sub>/hexane (1:1, v/v) as the eluent to give two separable bands.

The first, colorless, band was identified as Os(Cl)<sub>2</sub>(CO)<sub>2</sub>(PPh<sub>3</sub>)<sub>2</sub>, **4** (R<sub>f</sub> = 0.30; 3.0 mg, 30%). IR (CH<sub>2</sub>Cl<sub>2</sub>): ν(CO) 2044s, 1972s cm<sup>-1</sup>. <sup>1</sup>H NMR (C<sub>6</sub>D<sub>6</sub>) δ 8.13-8.19 (q, 12H, Ph-H), 6.90-7.01 (m, 18H, Ph-H). <sup>31</sup>P{<sup>1</sup>H} NMR (C<sub>6</sub>D<sub>6</sub>) δ -5.2 ppm. Anal. Calcd for C<sub>38</sub>H<sub>30</sub>Cl<sub>2</sub>O<sub>2</sub>OsP<sub>2</sub>: C 54.22, H 3.59. Found: C 54.13, H 3.36. ESI-MS<sup>+</sup> (m/z): 861 [M+H<sub>2</sub>O]<sup>+</sup>, 807 [M-Cl]<sup>+</sup>.

The second, nearly colorless, major band was identified as Os<sub>3</sub>(CO)<sub>10</sub>(PPh<sub>3</sub>)(SbPh)Cl<sub>2</sub>, **3** (R<sub>f</sub> = 0.20; yield = 15 mg, 64%). IR (CH<sub>2</sub>Cl<sub>2</sub>): ν(CO) 2133s, 2098s, 2058s, 2050s, 2032s, 1961m cm<sup>-1</sup>. <sup>1</sup>H NMR (C<sub>6</sub>D<sub>6</sub>) δ 7.95-8.01 (m, 6H, Ph-H), 7.64-7.66 (dd, 2H, Ph-H), 6.84-6.98 (m, 12H, Ph-H). <sup>31</sup>P{<sup>1</sup>H} NMR (C<sub>6</sub>D<sub>6</sub>) δ -9.5 ppm. Anal. Calcd for C<sub>34</sub>H<sub>20</sub>Cl<sub>2</sub>O<sub>10</sub>Os<sub>3</sub>PSb: C 29.53, H 1.46. Found: C 29.54, H 1.17. ESI-MS<sup>+</sup> (m/z): 1402 [M+H<sub>2</sub>O]<sup>+</sup>, 1349 [M-Cl]<sup>+</sup>.

**Reaction of 1 with one equivalent of Me<sub>3</sub>NO (TMNO)/CH<sub>3</sub>CN in the presence of PPh<sub>3</sub>.** A sample of **1** (20 mg, 17 μmol) and PPh<sub>3</sub> (27 mg, 102 μmol) were dissolved in dry dichloromethane (10 mL). A TMNO/CH<sub>3</sub>CN solution (1 mg/ml, 1.3 ml) was added dropwise over three minutes with stirring. After stirring for 30 minutes, the solvent was removed and the solid was dissolved in dichloromethane. TLC was carried out with DCM/hexane (2:1, v/v) as the mobile phase. Five bands were isolated (exclusive of the top colorless band identified as excess PPh<sub>3</sub>), out of which two were identified.

Band 1, pale yellow, was identified as Os<sub>2</sub>(CO)<sub>7</sub>(CH<sub>3</sub>CN)(μ<sub>3</sub>-SbPh)Os(CO)<sub>2</sub>(PPh<sub>3</sub>)Cl<sub>2</sub>, **5a** (R<sub>f</sub> = 0.27; yield = 5.2 mg, 14 %). IR (CH<sub>2</sub>Cl<sub>2</sub>): ν(CO) 2110m, 2063s, 2033s, 2004w, 1986w, 1958m cm<sup>-1</sup>. <sup>1</sup>H NMR (C<sub>6</sub>D<sub>6</sub>) δ 7.90-7.95 (m, 6H, Ph-H), 7.83-7.86 (dd, 2H, Ph-H), 6.88-7.03 (m, 12H, Ph-H), 1.44 (s, 3H, CH<sub>3</sub>CN). <sup>31</sup>P{<sup>1</sup>H} NMR (CDCl<sub>3</sub>) δ -4.8 ppm. Anal. Calcd for C<sub>35</sub>H<sub>23</sub>Cl<sub>2</sub>NO<sub>9</sub>Os<sub>3</sub>PSb: C 30.12, H 1.66. Found: C 30.25, H 1.41. ESI-MS<sup>+</sup> (m/z): 1415 [M+H<sub>2</sub>O]<sup>+</sup>, 1319 [M-Cl-CH<sub>3</sub>CN]<sup>+</sup>.

Band 2, pale yellow, was identified as Os<sub>3</sub>(CO)<sub>10</sub>(PPh<sub>3</sub>)(SbPh)Cl<sub>2</sub>, **3** (R<sub>f</sub> = 0.20; yield = 2.6 mg, 7 %).

Band 3, yellow, was not identified. R<sub>f</sub> = 0.14; yield = 1.9 mg. IR (CH<sub>2</sub>Cl<sub>2</sub>): ν(CO) 2107m, 2068m, 2039s, 2010m cm<sup>-1</sup>. Band 4, yellow, was not identified. R<sub>f</sub> = 0.10; yield = 1.4 mg. IR (CH<sub>2</sub>Cl<sub>2</sub>): ν(CO) 2135w, 2111m, 2099m, 2063s, 2033s, 2019s, 1987m, 1944m cm<sup>-1</sup>. Band 5, yellow, was not identified. R<sub>f</sub> = 0.05; yield = 3.9 mg. IR (CH<sub>2</sub>Cl<sub>2</sub>): ν(CO) 2109m, 2066m, 2037m, 2026s, 2007m, 1957w cm<sup>-1</sup>.

**Reaction of 1 with two equivalents of TMNO/CH<sub>3</sub>CN in the presence of PPh<sub>3</sub>.** A similar procedure to that in the case of one equivalent of TMNO was used and only the amount of TMNO was changed to two equivalents. Three bands were isolated after TLC separation.

Band 1, pale yellow, was identified as Os<sub>2</sub>(CO)<sub>7</sub>(CH<sub>3</sub>CN)(μ<sub>3</sub>-SbPh)Os(CO)<sub>2</sub>(PPh<sub>3</sub>)Cl<sub>2</sub>, **5a** (R<sub>f</sub> = 0.40; yield = 7 mg, 27%).

Band 2, pale yellow, was tentatively identified as Os<sub>2</sub>(CO)<sub>6</sub>(CH<sub>3</sub>CN)<sub>2</sub>(μ<sub>3</sub>-SbPh)Os(CO)<sub>2</sub>(PPh<sub>3</sub>)Cl<sub>2</sub>, **6a** (R<sub>f</sub> = 0.25; yield = 1.5 mg, 6%). IR (CH<sub>2</sub>Cl<sub>2</sub>): ν(CO) 2067m, 2040vs, 2024w, 1986m 1961sh, 1950sh cm<sup>-1</sup>; <sup>1</sup>H NMR (CD<sub>3</sub>CN) δ 1.42 (s, 3H, CH<sub>3</sub>CN), 2.26 (s, 3H, CH<sub>3</sub>CN), 7.17-7.20 (m, 3H, Ph-H), 7.41-7.45 (m, 12H, Ph-H), 7.57-7.59 (dd, 2H, Ph-H), 7.78-7.83 (m, 6H, Ph-H). <sup>31</sup>P{<sup>1</sup>H} NMR (CDCl<sub>3</sub>) δ -4.9 ppm. Anal. Calcd for C<sub>36</sub>H<sub>26</sub>Cl<sub>2</sub>N<sub>2</sub>O<sub>8</sub>Os<sub>3</sub>PSb: C 30.69, H 1.86. Found: C 30.86, H 1.72. ESI-MS<sup>+</sup> (m/z): 1428 [M+H<sub>2</sub>O]<sup>+</sup>, 1369 [M-CH<sub>3</sub>CN]<sup>+</sup>, 1334 [M-Cl-CH<sub>3</sub>CN]<sup>+</sup>.

Band 2, pale yellow, was tentatively identified as Os<sub>2</sub>(CO)<sub>6</sub>(CH<sub>3</sub>CN)<sub>2</sub>(μ<sub>3</sub>-SbPh)Os(CO)<sub>2</sub>(PPh<sub>3</sub>)Cl<sub>2</sub>, **6b** (R<sub>f</sub> = 0.16; yield = 1.0 mg, 4%). IR (CH<sub>2</sub>Cl<sub>2</sub>): ν(CO) 2111m, 2065s, 2035s, 2019s, 1986m cm<sup>-1</sup>; <sup>1</sup>H NMR (C<sub>6</sub>D<sub>6</sub>) δ 1.44 (s, 3H, CH<sub>3</sub>CN), 1.54 (s, 3H, CH<sub>3</sub>CN), 6.93-6.98 (m, 9H, Ph-H), 7.04-7.08 (t, 3H, Ph-H),

7.79–7.82 (dd, 2H, Ph-H), 7.99–8.05 (m, 6H, Ph-H).  $^{31}\text{P}\{^1\text{H}\}$  NMR ( $\text{CDCl}_3$ )  $\delta$  -5.9 ppm. Anal. Calcd for  $\text{C}_{36}\text{H}_{26}\text{Cl}_2\text{N}_2\text{O}_8\text{Os}_3\text{Psb}$ : C 30.69, H 1.86. Found: C 30.93, H 1.93. ESI-MS $^+$  (m/z): 1428  $[\text{M}+\text{H}_2\text{O}]^+$ , 1369  $[\text{M}-\text{CH}_3\text{CN}]^+$ , 1334  $[\text{M}-\text{Cl}-\text{CH}_3\text{CN}]^+$ .

Band 3, pale yellow, was tentatively identified as  $\text{Os}_2(\text{CO})_7(\text{CH}_3\text{CN})(\mu_3\text{-SbPh})\text{Os}(\text{CO})_2(\text{PPh}_3)_2\text{Cl}_2$ , **5b** ( $R_f = 0.10$ ; yield = 4.5 mg, 18%). IR ( $\text{CH}_2\text{Cl}_2$ ):  $\nu(\text{CO})$  2110m, 2065s, 2026br, 2007m, 1987m, 1957m  $\text{cm}^{-1}$ ;  $^1\text{H}$  NMR ( $\text{C}_6\text{D}_6$ )  $\delta$  2.18 (s, 3H,  $\text{CH}_3\text{CN}$ ), 6.89–6.99 (m, 12H, Ph-H), 7.65–7.67 (dd, 2H, Ph-H), 8.00–8.09 (m, 6H, Ph-H).  $^{31}\text{P}\{^1\text{H}\}$  NMR ( $\text{CDCl}_3$ )  $\delta$  -6.2 ppm. Anal. Calcd for  $\text{C}_{35}\text{H}_{23}\text{Cl}_2\text{NO}_9\text{Os}_3\text{Psb}$ : C 30.12, H 1.66. Found: C 30.06, H 1.52. ESI-MS $^+$  (m/z): 1415  $[\text{M}+\text{H}_2\text{O}]^+$ , 1319  $[\text{M}-\text{Cl}-\text{CH}_3\text{CN}]^+$ .

**Reaction of 1 with three equivalents of TMNO/ $\text{CH}_3\text{CN}$  in the presence of  $\text{PPh}_3$ .** A similar procedure to that in the case of one equivalent of TMNO was used and only the amount of TMNO was changed to three equivalents. Four bands were isolated after TLC separation.

Band 1, pale yellow, was tentatively identified as impure  $\text{Os}_2(\text{CO})_6(\text{PPh}_3)(\text{CH}_3\text{CN})(\mu_3\text{-SbPh})\text{Os}(\text{CO})_2(\text{PPh}_3)_2\text{Cl}_2$ , **6-P** ( $R_f = 0.49$ ; yield < 3 mg, < 11%). IR ( $\text{CH}_2\text{Cl}_2$ ):  $\nu(\text{CO})$  2094w, 2043m, 2022s, 1999s, 1975m, 1953m  $\text{cm}^{-1}$ . ESI-MS $^+$  (m/z): 1631  $[\text{M}]^+$ , 1649  $[\text{M}+\text{H}_2\text{O}]^+$ . The  $^1\text{H}$  NMR spectrum suggests that it is impure, and the mass spectrum suggests that some tetra-substituted product **7-P** is probably present (Figure S17).

Band 2, pale yellow, was tentatively identified as  $\text{Os}_2(\text{CO})_5(\text{PPh}_3)(\text{CH}_3\text{CN})_2(\mu_3\text{-SbPh})\text{Os}(\text{CO})_2(\text{PPh}_3)_2\text{Cl}_2$ , **7b** ( $R_f = 0.43$ ; yield = 2.9 mg, 10%). IR ( $\text{CH}_2\text{Cl}_2$ ):  $\nu(\text{CO})$  2042s, 2020m, 1995s, 1960m 1948sh  $\text{cm}^{-1}$ ;  $^1\text{H}$  NMR ( $\text{CD}_3\text{CN}$ )  $\delta$  0.91 (d, 3H,  $^5J_{\text{PH}} = 0.8$  Hz,  $\text{CH}_3\text{CN}$ ), 2.31 (s, 3H,  $\text{CH}_3\text{CN}$ ), 6.83–6.87 (t, 2H, Ph-H), 6.91–6.99 (m, 3H, Ph-H), 7.43–7.57 (m, 18H, Ph-H), 7.77–7.83 (m, 6H, m, Ph-H), 7.89–7.94 (m, 6H, Ph-H). Anal. Calcd for  $\text{C}_{53}\text{H}_{41}\text{Cl}_2\text{N}_2\text{O}_7\text{Os}_3\text{P}_2\text{Sb}\cdot 0.8\text{CH}_2\text{Cl}_2$ : C 37.76, H 2.51. Found: C 37.90, H 2.41. ESI-MS $^+$  (m/z): 1644  $[\text{M}]^+$ , 1604  $[\text{M}-\text{CH}_3\text{CN}]^+$ , 1562  $[\text{M}-2\text{CH}_3\text{CN}]^+$ .

Band 3, pale yellow, was identified as  $\text{Os}_2(\text{CO})_5(\text{PPh}_3)(\text{CH}_3\text{CN})_2(\mu_3\text{-SbPh})\text{Os}(\text{CO})_2(\text{PPh}_3)_2\text{Cl}_2$ , **7a** ( $R_f = 0.37$ ; yield = 8.0 mg, 28%). IR ( $\text{CH}_2\text{Cl}_2$ ):  $\nu(\text{CO})$  2044s, 2020m, 1988s, 1970m, 1948m 1927w  $\text{cm}^{-1}$ ;  $^1\text{H}$  NMR ( $\text{CD}_3\text{CN}$ )  $\delta$  1.32 (s, 3H,  $\text{CH}_3\text{CN}$ ), 1.68 (d, 3H,  $^5J_{\text{H-P}} = 0.8$  Hz,  $\text{CH}_3\text{CN}$ ), 6.82–6.85 (4H, m, Ph-H), 6.93–6.97 (m, 1H, Ph-H), 7.39–7.51 (m, 18H, Ph-H), 7.77–7.85 (m, 12H, Ph-H). Anal. Calcd for  $\text{C}_{53}\text{H}_{41}\text{Cl}_2\text{N}_2\text{O}_7\text{Os}_3\text{P}_2\text{Sb}$ : C 38.74, H 2.52. Found: C 39.15, H 2.73. ESI-MS $^+$  (m/z): 1644  $[\text{M}]^+$ , 1604  $[\text{M}-\text{CH}_3\text{CN}]^+$ , 1562  $[\text{M}-2\text{CH}_3\text{CN}]^+$ .

Band 4, pale yellow, was identified as **6a** ( $R_f = 0.24$ ; yield = 2.6 mg, 9%).

**Reaction of 1 with four equivalents of TMNO/ $\text{CH}_3\text{CN}$  in the presence of  $\text{PPh}_3$ .** A similar procedure to that in the case of one equivalent of TMNO was used and only the amount of TMNO was changed to four equivalents. Two major pale-yellow bands were isolated after TLC separation. Band 1 was identified as **7b** ( $R_f = 0.28$ ; yield = 1.9 mg, 7%) and band 2 was identified as **7a** ( $R_f = 0.22$ ; yield = 2.3 mg, 8%).

**Conversion of 7a to 7-P.** Cluster **7a** (8.0 mg, 4.9  $\mu\text{mol}$ ) was dissolved in 5 ml dry DCM, followed by addition of  $\text{PPh}_3$  (1.5 mg, 5.7  $\mu\text{mol}$ ). The mixture was stirred at room temperature for 2h. IR of the crude showed that **7a** was partly consumed and the crude solution was subject to mass detection to confirm the presence/formation of **7-P**.

**Conversion of 6a to 6-P and then to 7a.** The conversion of **6a** to **6-P** was examined in the same way as above but the reaction was found to proceed faster; after stirring at room temperature for 2h, IR showed **6a** was fully depleted and mass spectrum of the crude confirmed the presence/formation of **6-P**. One equivalent of TMNO solution in  $\text{CH}_3\text{CN}$  (1mg/ml) was then dropwise added and the resulting solution was further stirred at room tempera-

ture for 30 min; mass spectrum of the crude confirmed the presence/formation of **7a**.

**Generation and trapping of 2- $\text{CH}_3\text{CN}$ .** a) **Formation of  $\text{Os}_2(\text{CO})_7(\text{CH}_3\text{CN})(\mu_3\text{-SbPh})\text{Os}(\text{CO})_3\text{Cl}_2$ , **B**.** To a stirred solution of **1** (40 mg, 34  $\mu\text{mol}$ ) in dry  $\text{CH}_2\text{Cl}_2$  (15 mL) was added TMNO/ $\text{CH}_3\text{CN}$  solution (1 mg/ml, 5.3 ml) dropwise. After the IR spectrum showed that **1** has been consumed (~30 mins), the solution was first degassed through three freeze-pump-thaw cycles and then filled with CO gas. The resulting mixture was stirred at room temperature for another 10 h. The mass spectrum showed peaks ascribable to  $[\text{M}+\text{H}_2\text{O}]^+$ , albeit of low intensity, together with strong fragmentation peaks consistent with the formulation for **B**. b) **In-situ generation of 2- $\text{CH}_3\text{CN}$  and conversion to **8**.** The solvents from the above were removed *in vacuo* and the residue containing **B** redissolved in dry THF (15 ml). Neutral  $\gamma\text{-Al}_2\text{O}_3$  (700 mg) was added and the suspension was stirred for 30 min. A sample of  $\text{W}(\text{CO})_5(\text{NCCH}_3)$  (17 mg, 47  $\mu\text{mol}$ ) was then and after further stirring at room temperature for 12 h, the solvents were then removed and the residue separated by TLC with  $\text{CH}_2\text{Cl}_2$ /hexane (1:1, v/v) as the eluent to give three bands.

Band 1, pale yellow, was identified as  $\text{Os}_2(\text{CO})_7(\text{CH}_3\text{CN})(\mu_3\text{-SbPh})\text{W}(\text{CO})_5$ , **8a** ( $R_f = 0.65$ ; yield = 6 mg, 16%). IR ( $\text{CH}_2\text{Cl}_2$ ):  $\nu(\text{CO})$  2107m, 2057s, 2031m, 2023m, 2002w, 1982w, 1928s  $\text{cm}^{-1}$ ;  $^1\text{H}$  NMR ( $\text{CDCl}_3$ )  $\delta$  2.49 (s, 3H,  $\text{CH}_3\text{CN}$ ), 7.14–7.22 (m, 3H, Ph-H), 7.43 (d, 2H, Ph-H). Anal. Calcd for  $\text{C}_{20}\text{H}_8\text{NO}_{12}\text{Os}_2\text{WSb}$ : C 21.07, H 0.71. Found: C 20.84, H 1.12. ESI-MS $^+$  (m/z): 1141  $[\text{M}]^+$ , 1072  $[\text{M}-\text{CO}-\text{CH}_3\text{CN}]^+$ .

Band 2, pale yellow, was identified as  $\text{Os}_2(\text{CO})_7(\text{CH}_3\text{CN})(\mu_3\text{-SbPh})\text{W}(\text{CO})_5$ , **8b** ( $R_f = 0.60$ ; yield = 4 mg, 11%). IR ( $\text{CH}_2\text{Cl}_2$ ):  $\nu(\text{CO})$  2106m, 2062sh, 2056s, 2031sh, 2021s, 2006w, 1982w, 1930s  $\text{cm}^{-1}$ ;  $^1\text{H}$  NMR ( $\text{CDCl}_3$ )  $\delta$  1.67 (s, 3H,  $\text{CH}_3\text{CN}$ ), 7.16–7.31 (m, 3H, Ph-H), 7.38 (d, 2H, Ph-H). Anal. Calcd for  $\text{C}_{20}\text{H}_8\text{NO}_{12}\text{Os}_2\text{WSb}$ : C 21.07, H 0.71. Found: C 21.53, H 1.01. ESI-MS $^+$  (m/z): 1141  $[\text{M}]^+$ , 1072  $[\text{M}-\text{CO}-\text{CH}_3\text{CN}]^+$ .

Band 3, pale yellow, was identified as  $\text{Os}_2(\text{CO})_6(\text{CH}_3\text{CN})_2(\mu_3\text{-SbPh})\text{Os}(\text{CO})_3\text{Cl}_2$ , **9** ( $R_f = 0.55$ ; yield = 1 mg, 2.5%). It was only characterized crystallographically.

**Crystallographic analyses.** Diffraction-quality crystals were obtained by slow evaporation of  $\text{CH}_2\text{Cl}_2$ /hexane solutions. The X-ray diffraction intensity data were collected on a Bruker Kappa diffractometer equipped with a CCD detector, using Mo  $K_\alpha$  radiation ( $\lambda = 0.71073$  Å) except for **5** which was collected with Cu  $K_\alpha$  radiation ( $\lambda = 1.54178$  Å), with the SMART suite of programs [14]; the data were processed and corrected for Lorentz and polarization effects with SAINT and for absorption effects with SADABS [15]. All the structural solutions and refinements were performed with the SHELXTL suite of programs [16]. All non-hydrogen atoms were refined with anisotropic thermal parameters. Crystal data, data collection parameters, and refinement data are summarized in Table 2.

The crystal of **9** was refined as a racemic twin. The molecule of **4** sits on an inversion centre and exhibits disorder of one CO/Cl. The crystal of **3** contains two  $\text{CH}_2\text{Cl}_2$  solvates, one with half occupancy and the other disordered. The crystal of **7a** also contains two DCM solvates, with one disordered. Both disordered solvates were modelled with two sites each. Appropriate restraints were placed on all disordered parts.

**Computational studies.** DFT calculations were carried out with the Gaussian 09W suite of programs [17], employing Becke's three-parameter hybrid function and Lee-Yang-Parr's gradient-corrected correlation function (B3LYP) [18]. The LANL2DZ basis set [19], together with d- or f-type polarization functions [20], was employed for the Os and Sb atoms, while the 6-311+G (2d, p) basis set was used for the lighter atoms. Spin-restricted calculations were used for geometry optimizations, Gibbs free energy calculations and natural bonding orbital (NBO) analysis. Harmonic frequencies were

**Table 2**  
Crystallographic data for compounds **3**, **3'**, **4**, **5a**, **7a**, **8a**, **8b** and **9**.

Compound	3'	3	4	5a
Empirical formula	C <sub>19</sub> H <sub>14</sub> Cl <sub>2</sub> O <sub>10</sub> Os <sub>3</sub> PSb	C <sub>34</sub> H <sub>20</sub> Cl <sub>2</sub> O <sub>10</sub> Os <sub>3</sub> PSb• 0.5CH <sub>2</sub> Cl <sub>2</sub>	C <sub>38</sub> H <sub>30</sub> Cl <sub>2</sub> O <sub>2</sub> OsP <sub>2</sub>	C <sub>35</sub> H <sub>23</sub> Cl <sub>2</sub> NO <sub>9</sub> Os <sub>3</sub> PSb
Formula weight	1196.52	1425.18	841.66	1395.76
Temperature (K)	100(2)	153(2)	103(2)	123(2)
Crystal system	Triclinic	Monoclinic	Monoclinic	Triclinic
Space group	P $\bar{1}$	P2 <sub>1</sub> /c	C2/c	P $\bar{1}$
a (Å)	9.4181(2)	16.8324(13)	24.2073(10)	8.2644(2)
b (Å)	17.0852(4)	16.4156(13)	9.4316(5)	10.2258(3)
c (Å)	18.0483(4)	29.698(3)	15.7875(9)	24.6754(6)
$\alpha$ (deg)	97.7822(8)	90.00	90	79.5777(11)
$\beta$ (deg)	97.4944(8)	91.361(2)	116.095(4)	87.8297(10)
$\gamma$ (deg)	93.4340(8)	90.00	90	68.6405(10)
V (Å <sup>3</sup> )	2843.92(11)	8203.6(11)	3237.1(3)	1909.15(9)
Z value	4	8	4	2
$\rho_{\text{calc}}$ (g/cm <sup>3</sup> )	2.795	2.308	1.727	2.428
$\mu$ (Mo K $\alpha$ ) (mm <sup>-1</sup> )	14.591	10.200	4.238	26.078
F(000)	2144	5224	1656	1280
Crystal size, mm <sup>3</sup>	0.058 × 0.187 × 0.190	0.28 × 0.18 × 0.16	0.30 × 0.20 × 0.16	0.02 × 0.04 × 0.16
2 $\theta$ max (°)	26.37	26.37	28.40	66.98
Reflections collected	75638	91519	77103	62985
Independent reflections	11639 [R(int) = 0.0475]	16451 [R(int) = 0.0708]	4062 [R(int) = 0.0499]	6738 [R(int) = 0.0480]
Max. and min. transmission	0.4850 and 0.1680	0.29 and 0.16	0.5504 and 0.3629	0.62 and 0.27
Data/parameters	11639 / 655	16451/978	4062/219	6738/470
Goodness of fit on F <sup>2</sup>	1.057	1.062	1.063	1.255
Final R indices [I>2 $\sigma$ (I)]	R1 = 0.0211 wR2 = 0.0418	R1 = 0.0640 wR2 = 0.1404	R1 = 0.0161 wR2 = 0.0386	R1 = 0.0284 wR2 = 0.0706
R indices (all data)	R1 = 0.0275 wR2 = 0.0444	R1 = 0.0797 wR2 = 0.1502	R1 = 0.0179 wR2 = 0.0398	R1 = 0.0285 wR2 = 0.0706
Largest diff. peak and hole (e $\cdot$ Å <sup>-3</sup> )	1.672 and -1.012	3.050 and -3.178	0.589 and -0.449	1.197 and -1.570
<b>Table 2</b> (continued)				
Compound	7a	8a	8b	9
Empirical formula	C <sub>53</sub> H <sub>41</sub> Cl <sub>2</sub> N <sub>2</sub> O <sub>7</sub> Os <sub>3</sub> P <sub>2</sub> Sb• 2CH <sub>2</sub> Cl <sub>2</sub>	C <sub>20</sub> H <sub>8</sub> NO <sub>12</sub> Os <sub>2</sub> SbW	C <sub>20</sub> H <sub>8</sub> NO <sub>12</sub> Os <sub>2</sub> SbW	C <sub>19</sub> H <sub>11</sub> Cl <sub>2</sub> N <sub>2</sub> O <sub>9</sub> Os <sub>3</sub> Sb
Formula weight	1812.92	1140.27	1140.27	1174.55
Temperature (K)	103(2)	103(2)	103(2)	100(2)
Crystal system	Triclinic	Monoclinic	Triclinic	Monoclinic
Space group	P $\bar{1}$	P2 <sub>1</sub> /n	P $\bar{1}$	Cc
a (Å)	14.3957(5)	9.3714(3)	9.1224(2)	11.6971(5)
b (Å)	15.7081(6)	16.8083(6)	9.2835(2)	14.2259(6)
c (Å)	16.2226(6)	16.9781(6)	16.1604(4)	16.3751(6)
$\alpha$ (deg)	116.615(2)	90	95.1604(9)	90
$\beta$ (deg)	96.625(2)	91.9450(14)	97.6992(9)	91.4623(15)
$\gamma$ (deg)	109.653(2)	90	103.7537(8)	90
V (Å <sup>3</sup> )	2930.4(2)	2672.80(16)	1306.77(5)	2723.96(19)
Z value	2	4	2	4
$\rho_{\text{calc}}$ (g/cm <sup>3</sup> )	2.055	2.834	2.898	2.864
$\mu$ (Mo K $\alpha$ ) (mm <sup>-1</sup> )	7.319	14.826	15.162	15.174
F(000)	1712	2032	1016	2096
Crystal size, mm <sup>3</sup>	0.10 × 0.08 × 0.04	0.10 × 0.12 × 0.16	0.12 × 0.15 × 0.21	0.06 × 0.24 × 0.32
2 $\theta$ max (°)	31.22	26.37	25.35	30.55
Reflections collected	75123	5454	4782	25494
Independent reflections	18947 [R(int) = 0.0673]	5454	4782	8092 [R(int) = 0.0644]
Max. and min. transmission	0.76 and 0.50	0.319 and 0.200	0.255 and 0.144	0.463 and 0.0852
Data/parameters	18947/693	5454/335	4782/355	8092/327
Goodness of fit on F <sup>2</sup>	1.032	1.136	1.078	1.039
Final R indices [I>2 $\sigma$ (I)]	R1 = 0.0351 wR2 = 0.0645	R1 = 0.0273 wR2 = 0.0494	R1 = 0.0213 wR2 = 0.0403	R1 = 0.0362 wR2 = 0.0702
R indices (all data)	R1 = 0.0651 wR2 = 0.0756	R1 = 0.0350 wR2 = 0.0524	R1 = 0.0261 wR2 = 0.0420	R1 = 0.0422 wR2 = 0.0730
Largest diff. peak and hole (e $\cdot$ Å <sup>-3</sup> )	3.078 and -1.915	1.999 and -1.461	2.196 and -1.457	2.226 and -1.716

then calculated to characterize the stationary points as equilibrium structures with all real frequencies, and to evaluate zero-point energy (ZPE) corrections.

#### Supporting Information:

Crystallographic data for the structures in this paper have been deposited with the Cambridge Crystallographic Data Centre as supplementary publication numbers CCDC 2053892-6 and 2062344-6. Copies of the data can be obtained, free of charge, on application to CCDC, 12 Union Road, Cambridge CB2 1EZ, UK, (fax: +44 1223 336033 or e-mail: deposit@ccdc.cam.ac.uk). The <sup>1</sup>H, <sup>31</sup>P, IR and MS spectra of the new compounds, ORTEP diagrams and selected bond parameters of **3'** and **4**, and all the computationally optimized structures.

#### Declaration of Competing Interest

The authors declare that they have no known competing financial interests or personal relationships that could have appeared to influence the work reported in this paper.

#### Acknowledgment

This research is supported by the Ministry of Education, Singapore, under its Academic Research Fund Tier 1 (Project ID RG15/17) and Seed Funding from the Nanyang Technological University, as well as the National Natural Science Foundation of China (Grant No. 22001139) and the Natural Science Foundation of Shandong Province (Grant No. ZR2019BB058). The authors also acknowledge

the financial support from Program for Scientific Research Innovation Team in Colleges and Universities of Shandong Province.

### Supplementary materials

Supplementary material associated with this article can be found, in the online version, at doi:10.1016/j.jorganchem.2021.121817.

### References

- [1] E.C. Constable, C.E. Housecroft, in: *Comprehensive Inorganic Chemistry II*, 2nd Edition, Elsevier, Amsterdam, 2013, pp. 1–29.
- [2] J. Bauer, H. Braunschweig, R.D. Dewhurst, *Chem. Rev.* 112 (2012) 4329–4346.
- [3] J. Takaya, *Chem. Sci.* 12 (2021) 1964–1981.
- [4] D. You, F.P. Gabbai, *Trends Chem.* 1 (2019) 485–496.
- [5] (a) Y.-Z. Li, R. Ganguly, W.K. Leong, *Organometallics* 33 (2014) 3867–3876; (b) Y.-Z. Li, R. Ganguly, W.K. Leong, *Eur. J. Inorg. Chem.* (2017) 2541–2546.
- [6] Y.-Z. Li, R. Ganguly, D.R. Rajaratnam, W.K. Leong, *J. Organomet. Chem.* 858 (2018) 53–61.
- [7] (a) A.H. Cowley, N.C. Norman, M. Pakulski, *J. Am. Chem. Soc.* 106 (1984) 6844–6845; (b) A.H. Cowley, N.C. Norman, M. Pakulski, D. Bricker, D.R. Russell, *J. Am. Chem. Soc.* 107 (1985) 8211–8218.
- [8] Y.-Z. Li, R. Ganguly, W.K. Leong, *J. Organomet. Chem.* 820 (2016) 46–54.
- [9] J. Shen, Y. Gao, Q. Shi, F. Basolo, *Inorg. Chem.* 27 (1988) 4236–4239.
- [10] A.K. Raha, S. Ghosh, M. Manzurul Karim, D.A. Tocher, N. Begum, A. Sharmin, E. Rosenberg, S.E. Kabir, *J. Organomet. Chem.* 693 (2008) 3613–3621.
- [11] (a) C.K. McClure, In *Encyclopedia of Spectroscopy and Spectrometry*; Lindon, J. C., Eds.; Elsevier: Oxford, 1999, pp 2234–2245; (b) C.W. Anson, D.M. Thamattoor, *J. Org. Chem.* 77 (2012) 1693–1700.
- [12] (a) E. Rüba, W. Simanko, K. Mauthner, K.M. Soldouzi, C. Slugovc, K. Mereiter, R. Schmid, K. Kirchner, *Organometallics* 28 (1999) 3843–3850; (b) C.K. Tseng, A. Mihailovski, *Org. Magn. Res.* 6 (1974) 494–496; (c) C.E. Griffin, M. Gordon, *J. Am. Chem. Soc.* 89 (1967) 4427–4431.
- [13] F. Nief, F. Mercier, F. Mathey, *J. Organomet. Chem.* 328 (1987) 349–355.
- [14] SMART version 5.628; Bruker AXS Inc.: Madison, WI, USA, 2001.
- [15] G.M. Sheldrick, *SADABS: Program for Empirical Absorption Correction of Area Detector Data*, University of Gottingen, Germany, 1996.
- [16] (a) G.M. Sheldrick, *SHELXTL version 5.1*, Bruker AXS Inc., Madison, WI, USA, 1997; (b) G.M. Sheldrick, *Crystal structure refinement with SHELXL*, 2015 Acta Crystallogr., Sect. C: Struct. Chem., C71 3–8.
- [17] Gaussian 09, Revision D.01, M.J. Frisch, G.W. Trucks, H.B. Schlegel, G.E. Scuseria, M.A. Robb, J.R. Cheeseman, G. Scalmani, V. Barone, B. Mennucci, G.A. Petersson, H. Nakatsuji, M. Caricato, X. Li, H.P. Hratchian, A.F. Izmaylov, J. Bloino, G. Zheng, J.L. Sonnenberg, M. Hada, M. Ehara, K. Toyota, R. Fukuda, J. Hasegawa, M. Ishida, T. Nakajima, Y. Honda, O. Kitao, H. Nakai, T. Vreven, J.A. Montgomery, Jr., J.E. Peralta, F. Ogliaro, M. Bearpark, J.J. Heyd, E. Brothers, K.N. Kudin, V.N. Staroverov, R. Kobayashi, J. Normand, K. Raghavachari, A. Rendell, J.C. Burant, S.S. Iyengar, J. Tomasi, M. Cossi, N. Rega, J.M. Millam, M. Klene, J.E. Knox, J.B. Cross, V. Bakken, C. Adamo, J. Jaramillo, R. Gomperts, R.E. Stratmann, O. Yazyev, A.J. Austin, R. Cammi, C. Pomelli, J.W. Ochterski, R.L. Martin, K. Morokuma, V.G. Zakrzewski, G.A. Voth, P. Salvador, J.J. Dannenberg, S. Dapprich, A.D. Daniels, Ö. Farkas, J.B. Foresman, J.V. Ortiz, J. Cioslowski, and D.J. Fox, Gaussian, Inc., Wallingford CT, 2009.
- [18] C. Lee, W. Yang, R.G. Parr, *Phys. Rev. B* 37 (1988) 785–789.
- [19] (a) P.J. Hay, W.R. Wadt, *J. Chem. Phys.* 82 (1985) 270–283; (b) W.R. Wadt, P.J. Hay, *J. Chem. Phys.* 82 (1985) 284–298.
- [20] S. Huzinaga, J. Andzelm, in: *Gaussian Basis Sets for Molecular Calculations*, Elsevier: Amsterdam, 1984, p. 23.